G M McCracken et al

Studies in JET Divertors of Varied Geometry III: Intrinsic Impurity Behaviour

Studies in JET Divertors of Varied Geometry III: Intrinsic Impurity Behaviour

G M McCracken, R Barnsley, H Y Guo, M von Hellermann, L D Horton, H J Jäckel, J Lingertat, C Maggi, G F Matthews, R D Monk, M G O'Mullane[1], M F Stamp, P C Stangeby[2], G C Vlases, K-D Zastrow.

JET Joint Undertaking, Abingdon, Oxfordshire, OX14 3EA,
[1] University of Strathclyde, Glasgow, G4 0NG, UK.
[2] University of Toronto, Institute for Aerospace Studies, M3H 5T6, Canada.

ABSTRACT

Impurity production and plasma impurity concentrations are surveyed over a wide range of operating conditions but with emphasis on ELMy H-mode operation using neutral beam heating. The Mk I divertor campaigns with carbon and beryllium targets are compared to the Mk II campaign which had carbon targets and a more closed divertor geometry. The beryllium target campaign has a significantly lower impurity level than those with carbon targets although the Z_{eff} is still dominated by carbon. The divertor geometry appears to have little effect on the impurity level but it is found that the ELM frequency has a marked effect on Z_{eff}, and the carbon and nickel concentrations, with maxima at an ELM frequency around 5-15 Hz. This occurs whether the ELM frequency is varied by changing the plasma triangularity, the input power or by increasing the fuelling rate. The absolute impurity influxes from the inner and outer target and from the inner wall have been estimated from the CII and CIII line intensities. These fluxes are compared to the central carbon concentration and an attempt is made to correlate the influxes and the concentrations in the confined plasma both in their time evolution and in their absolute values.

1. INTRODUCTION

Impurity production in tokamaks results from interaction of plasma with the walls, limiters and divertor targets. The two principal impurity production processes occurring in a well-conditioned vacuum vessel are physical and chemical sputtering [1,2,3]. Each depends on the flux, energy, mass and angular distribution of the incident species. In addition, chemical sputtering depends on the surface temperature. In order to predict the impurity content of a plasma for a given geometry and operating conditions it is necessary to know the flux and energy distribution of the plasma arriving at the wall and also the transport of the impurities from the source into the confined plasma. Unravelling these various processes is proving to be a formidable task [4-8]. One of the objectives of these studies is to deterrmine whether ITER will achieve the goal of limiting the impurity level to a $Z_{eff} < 1.6$ [9].

The general objective of installing divertors in tokamaks is to remove the region of interaction of the plasma with surfaces far from the confined plasma. Even with divertors the intrinsic impurity content of the plasma in current devices seems to be marginal for reactor operation and it is not clear how to scale from current devices to fusion reactors.

The JET programme has a series of divertors of increasingly closed geometry, from the open design first introduced in 1988 [10] to the Mk IIGB (gas box) planned for 1998 [11]. The original open divertor experiments in JET were carried out on the carbon tiles in the upper half of the vessel and on the beryllium tiles at the bottom. The first purpose-built divertor, Mk I, was installed in 1993-4 and operated in 1994-5 [12]. New poloidal coils were installed inside the vessel to give improved control of the positions of the x-point and the separatrix strike points on

the target tiles, fig 1a. The divertor geometry was relatively open allowing strike point sweeping. The tiles were mounted on a rigid frame and accurately aligned to reduce hot spots due to localized power deposition. It was operated first with graphite target plates (Mk IC) and later with Be targets (Mk IBe). Mark IIA was installed in 1995/6 and operated in the 1996 campaign [13]. The Mk II divertor is a more closed design than Mk I to reduce the flow of neutrals back into the confined plasma, fig 1b. It was thereby hoped to reduce the impurity production by charge exchange in the main chamber. The graphite target plates are domed and the vertical side plates moved in, parallel to the magnetic flux surfaces. The design allows the strike point either to be onthe "horizontal" or on the vertical side plates, as in MkI. Both the Mk I and the Mk IIA had fairly significant "bypass" leakage paths [13] which allowed gas to flow from the subdivertor region back into the main chamber. In Oct 1996 these bypasses were blocked to reduce the neutral gas backflow. Operation with Mk IIAP

Fig.1: Comparison of the JET Mk I (a) and Mk IIA (b) divertor geometries

(Plugged) started in Nov 1996 and is the present configuration. Although not a deliberate part of the design, the Mk II geometry limited the cooling of the divertor tiles and allowed them to operate at a base temperature of 500 K compared with the 300 K of Mk I tiles. In fact the impurity production yield at the target is about a factor of 2 higher in Mk II than in Mk I, while the Zeff and the radiated power (Prad) were not significantly changed. The detailed evidence for these effects and the conclusions are discussed.

In the present paper we attempt to summarize the results of a series of measurements of impurity fluxes and central impurity concentrations in a wide range of operating conditions in JET with different divertor configurations during the Mk I and Mk II divertor campaigns. An attempt is made to correlate the influxes and the concentrations in the confined plasma both in their time evolution and in their absolute values. It is found that while for a particular discharge the time correlations appear quite good the correlations of the absolute influxes with the central concentrations are weak. This analysis of the intrinsic impurities is a companion paper to one on density limits and confinement [14] and one discussing the behaviour of seeded impurities [15].
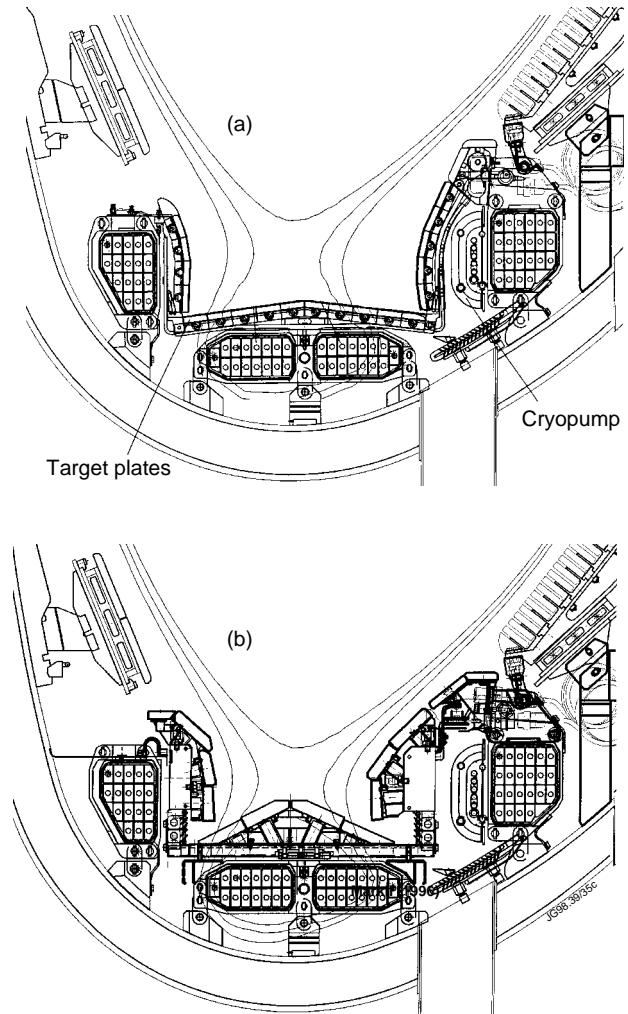
2

2. EXPERIMENTAL RESULTS

2.1. Global impurity measurements, Mk II divertor

The dominant intrinsic impurity in JET is carbon. During the early part of any campaign, particularly after a manned intervention into the vessel, other impurities such as oxygen and chlorine can contribute significantly to the radiated power. However after conditioning the Z_{eff} is normally accounted for by the carbon concentration. Although since 1989 beryllium has been evaporated routinely onto the main chamber and divertor surfaces as a getter and beryllium divertor target plates have been used [16], beryllium has never been the dominant impurity. Be gettering has the effect of reducing the oxygen to typically ~ 0.1%. The core carbon impurity concentration is usually in the 1 to 3% range, almost independent of operating conditions. A comparison of the operation with carbon and beryllium during the 1994-95 campaign with the Mk I divertor has been published [17]

   We first consider the parametric dependence of the global quantities Z_{eff} and P_{rad}. Data from different operating periods have been selected from the JET database. This database includes a large number of JET parameters, measured typically at 0.5 s intervals, coincident with the n_e and T_e measurements from the Thomson scattering diagnostic. The selection has been done on a number of criteria including, steady state conditions, $\dot{W}/P_T < 0.1$, (where P_T is the total input power and $\dot{W}$ is the rate of change of total stored energy), and with input power and plasma current between fixed limits. Other criteria such as plasma shape, specific shot range, etc. can be selected from the database at choice. The data so selected has been compared with the Divertor Task Force steady state ELMy H-mode database used in an earlier study [18]. In general they are in good agreement. However the previous data is rather sparse and since there is no significant reduction in data scatter we have generally used the larger data base. Z_{eff} is calculated from bremsstrahlung emission at 523 nm measured along both horizontal and vertical lines of sight through the centre of the plasma [19]. These are both line averaged measurements and are normally in good agreement. The total radiation is measured with a large number of lines of sight using thin gold foil bolometers of the ASDEX type [20].

   In MkIIA divertor operation, for a given volume averaged density, $^{TM}n_e$, Z_{eff} is almost independent of input power, fig 2a. The independence of power is at first sight rather surprising, especially as the range covered is from ohmic discharges with $P_T < 3$ MW, through L-mode to high power H-mode with $P_T \sim 16$ MW and with triangularity $0.15 < \delta < 0.25$. It must be related to the relative insensitivity of the sputtering yield to ion energy or to a compensating increase in the impurity screening as the density rises. It is not due to collinearity of the density with the input power since Z_{eff} for a narrow density range is also independent of input power, fig 2a. The total radiated power increases roughly linearly with input power, fig 2b. In these discharges with intrinsic impurities, the fraction of the total power that is radiated is $P_{rad}/P_T \approx 0.25$. The density dependence of Z_{eff} and P_{rad} for a range of powers are shown in fig 2c, 2d. There is a slight

tendency for Z_{eff} to decrease with increasing density for a given power. This has been more noticeable in other campaigns as discussed below. P_{rad} increases strongly with density. When data from all input powers is included the dependence is $\sim^{TM}n_e^2$. This result is consistent with the approximately constant Z_{eff}.
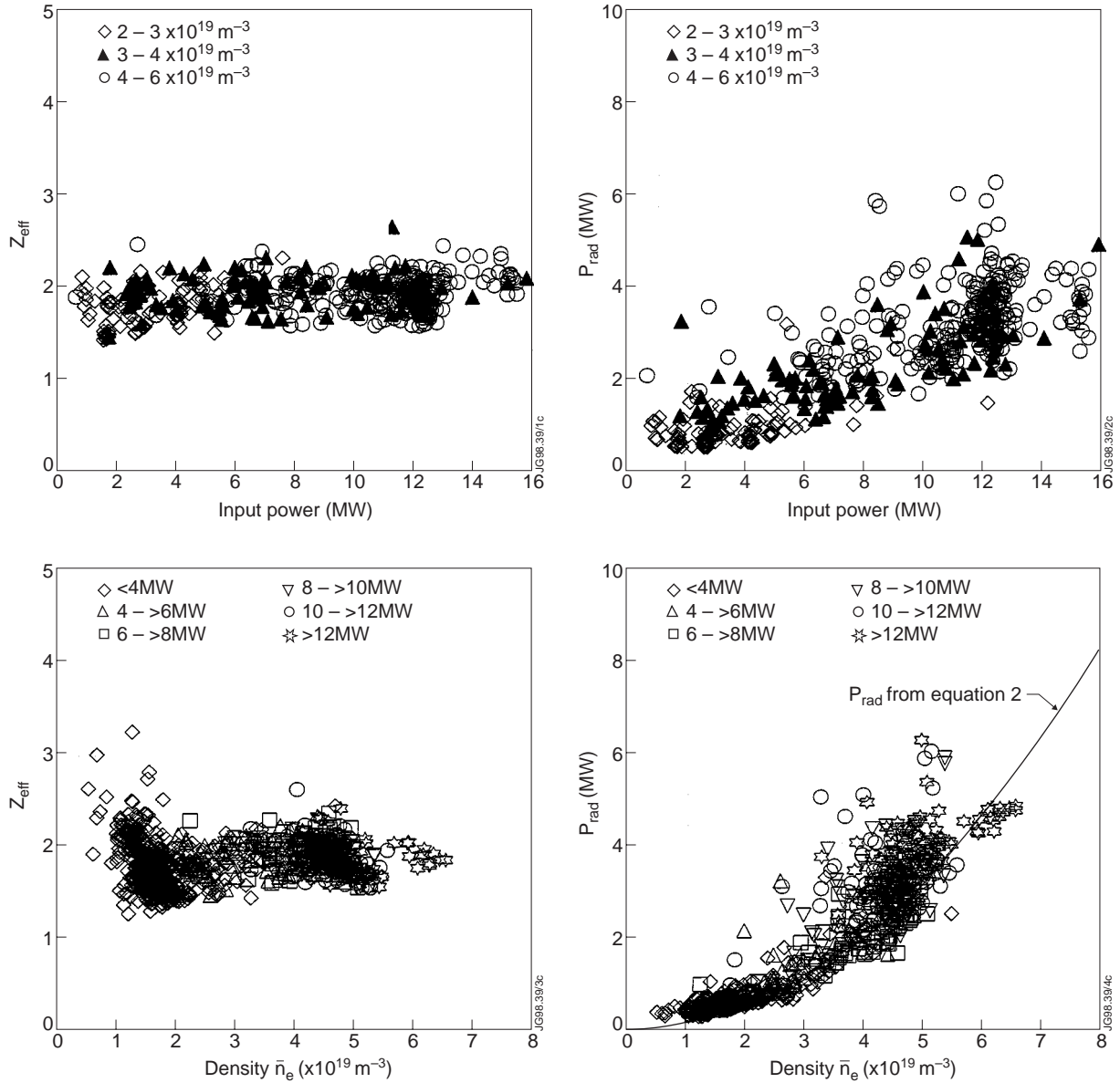

Fig.2: Parametric dependence of Z_{eff} and P_{rad} on total input power and core plasma density in JET diverted discharges with $2.4 < I_p < 2.7$ MA; ohmic and neutral beam heating only. Triangularity <0.25.

(a) Dependence of Z_{eff} on input power for various densities

(b) Dependence of P_{rad} on input power for various densities

(c) Dependence of Z_{eff} on volume average density for various input powers

(d) Dependence of P_{rad} on volume average density for various input powers

The solid curve is a fit from equation 2.

Measurements of the intrinsic impurity concentrations have been obtained for carbon, beryllium and helium with the charge exchange diagnostic (KS4) [21] and for nickel with the X-ray spectrometer (KX1) [22]. The carbon concentration is in the range 0.5 to 3%, fig. 3a, which usually accounts for most of the observed Z_{eff}. As with the Z_{eff} the carbon concentration appears to be weakly dependent on input power. The beryllium concentration, fig 3b, is ~20% of the carbon but because of the lower atomic number it contributes <10% of the Z_{eff}. Helium is frequently introduced into discharges for minority ICRF heating and is subsequently found at the 0.5 to 3% level. This makes a negligible contribution to the Z_{eff} and P_{rad}. The nickel concentration is normally less than 10^{-4} and thus also makes an insignificant contribution to both Z_{eff} and P_{rad}. Generally the carbon, beryllium and nickel densities increase with plasma density so that their concentrations are constant, fig 3. There is a slight apparent discrepancy between the sum of the carbon and beryllium contributions to the Z_{eff} and the value measured from the bremsstrahlung. This is partly because the Z_{eff} is a line averaged value while the concentrations are central values and the profiles are hollow. The average ratio of centre to edge concentration in beam heated discharges is 0.42±0.12. The carbon density profile is slightly less hollow because the electron density profile is peaked.
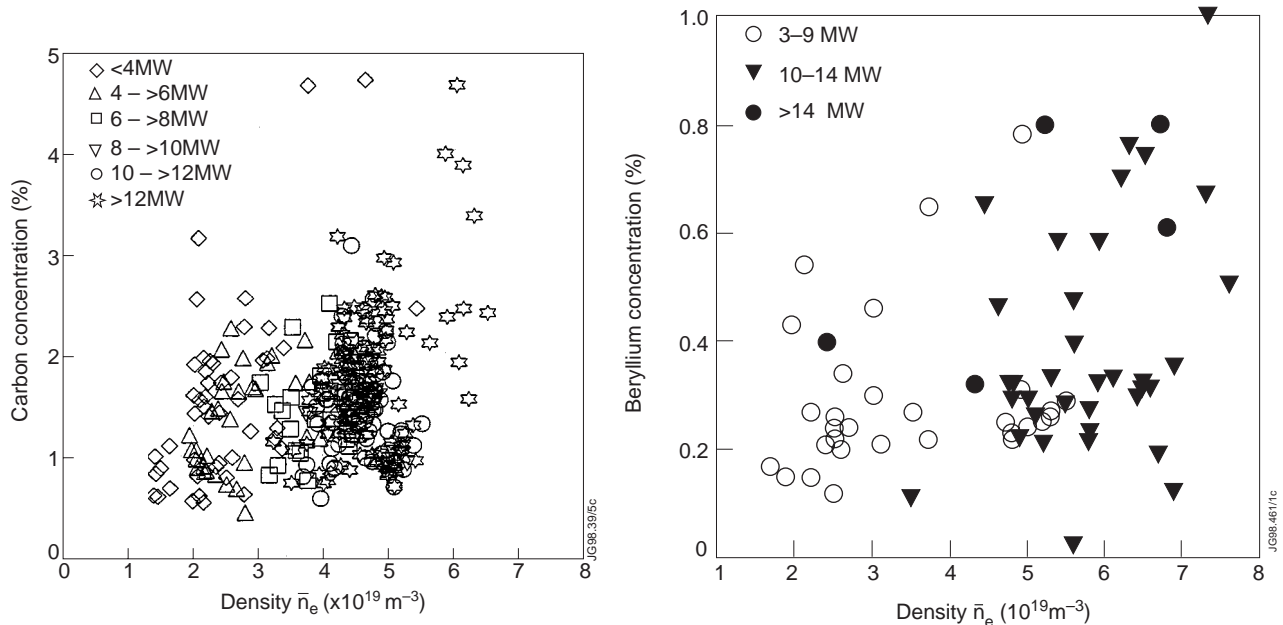

Fig.3: Impurity concentration at r/a=0.2 measured by charge exchange spectroscopy as a function of core plasma density for different input powers for the Mk II divertor.
$2.4 < I_p < 2.7$ MA; Triangularity <0.25. No ICRH or LH heating.
(a) Carbon (b) Beryllium

There are small contributions to Z_{eff} from beryllium and oxygen. The oxygen and chlorine concentrations are normally too small to be detected using the charge exchange diagnostic. However they are measured using a Bragg crystal spectrometer [23] (KS6) viewing the plasma across the midplane. The O VIII (1.90 nm), Cl XVI (4.48 nm) and C VI (3.35 nm) lines are routinely monitored. The ratios of the brightnesses of these lines for equal concentrations is

obtained from modelling. Because the ions observed occur at similar plasma temperatures and densities the relative brightnesses vary little with operating conditions and the relative concentrations can thus be derived. The oxygen/carbon and chlorine/carbon ratios increase to ~0.2 and ~ 0.04 respectively immediately after the vacuum vessel has been opened for maintenance, with a larger increase after a manned intervention, figs 4a and 4b. The carbon concentration normally changes by less than 50%. Chlorine and oxygen are removed by glow discharge cleaning, by beryllium evaporation and by routine tokamak operation over a period of 400 to 500 discharges. The clean up at the beginning of the 1996 campaign and again after a manned intervention is shown in figs 4a and 4b. The ratio of the oxygen/carbon density is typically ≤ 0.1 in well-conditioned discharges while the chlorine/carbon density ratio is ≤ 0.01, The corresponding contributions to Z_{eff}, relative to carbon, are < 0.2 and < 0.1 respectively.

2.2. Effect of configuration

A wide variety of configuration changes have been studied in JET, including changes in the plasma shape, such as triangularity and magnetic flux expansion (thus changing the parallel connection length to the divertor), to changes in the divertor geometry. There is no discernible effect in Z_{eff} or carbon concentration when changing the strike point position from horizontal to vertical target configuration or in changing the divertor flux expansion. However there is typically an increase of a factor 2 in the carbon concentration in changing from low to high triangularity. This change is correlated with the decrease in the ELM frequency and increase in ELM size observed in high triangularity discharges [13, 24]. The Z_{eff}, carbon and nickel concentrations are plotted as a function of ELM frequency in fig 5. There is a decrease of more than an order of magnitude in the nickel concentration as the ELM frequency increases from 5 Hz to 30 Hz, fig 5c. The same effect is seen in the carbon concentration but to a lesser degree, fig 5b. The effect is also observed in Z_{eff}, which falls from ~2.1 at 5 Hz to ~1.6 at 30 Hz., fig 5a. The ELM
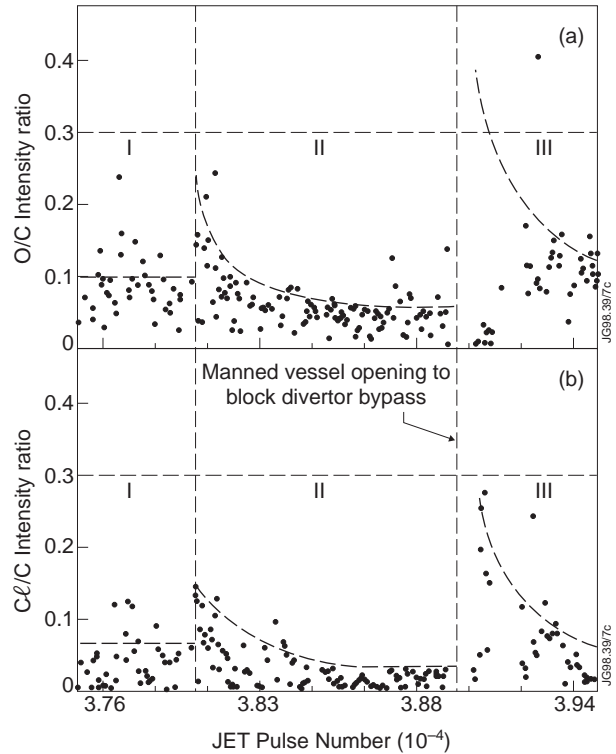

Fig.4: Ratio of (a) the O VIII and (b) the Cl XVI to C VI intensities during a diverted discharge at 53 s as a function of shot number. Measurements are from the X-ray crystal spectrometer (KS3) looking across the midplane radial view at the plasma. Period I is during the initial start up of the 1996 campaign after the installation of the Mk II divertor (15/7/96 to 5/8/96). Period II is during routine operation (5/8/96 to 28/9/96). Period III is after a manned intervention to block the divertor bypass leaks (2/11/96 to 30/11/96). The clean-up of the chlorine and oxygen takes 400-500 discharges. The dotted lines are only to guide the eye.
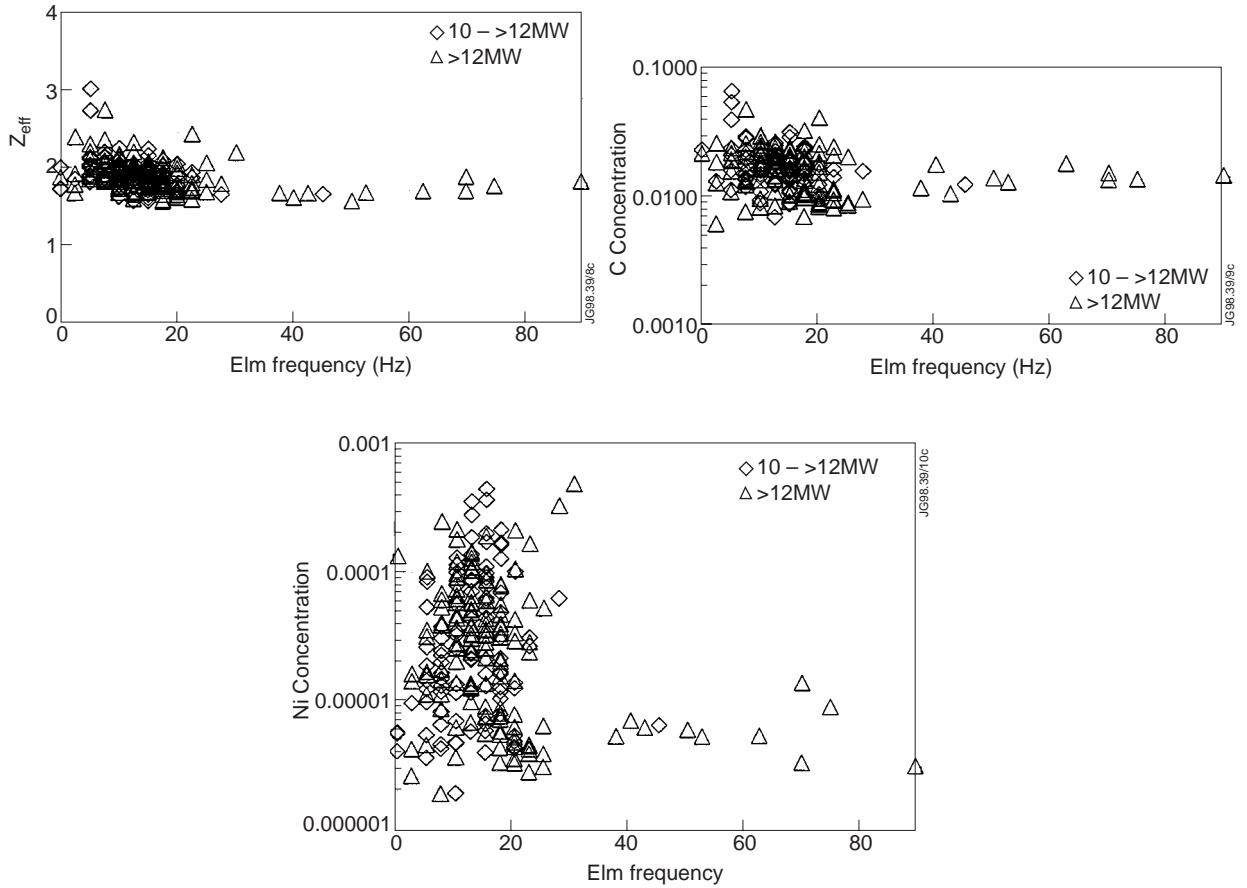
6

Fig.5: Dependence of core plasma parameters on ELM frequency in diverted ELMy H-mode discharges with $4 < \bar{n}_e < 6x10^{19}$ m^{-3}, $2.4 < I_p < 2.7$ MA; Triangularity <0.25. No ICRH or LH heating.
(a) Zeff;
(b) Carbon concentration at r/a=0.2;
(c) Nickel concentration at r/a~0.4

frequency can be increased in a number of ways, including decreasing the triangularity, increasing the gas puffing, increasing the input power or changing from hydrogen to deuterium and tritium plasmas. The effect on the impurities is independent of how the ELM frequency is changed. In the case of nickel there are clear signs of accumulation in the core between ELMs that is enhanced by the longer period between ELMs. The low ionization states are enhanced during the larger low frequency ELMs, possibly due to more nickel influx from the larger ELMs. Operation was mainly at low ELM frequency. At higher frequency the nickel concentration did not exceed $2x10^{-5}$.

In Mk I and the initial version of the Mk IIA there were significant gaps between the sub-divertor volume and the main chamber around the edge of the divertor structure. There was concern that these "bypasses" allowed excessive neutral gas flow from the divertor back into the main chamber which could contribute to impurity production by charge exchange in the plasma, leading to fast neutrals interacting with the wall of the main chamber. The increased sub-divertor pressure in Mk IIA relative to Mk I [13] forced more neutrals through the bypasses, tending to offset the reduction of neutral flow out of the divertor throat due to the more closed geometry of

Mk IIA. The bypass leaks were closed in October 1996 and the modified divertor, denoted Mk IIAP, then investigated. It was found that at a given density there was no measurable difference in the impurity level, estimated either by the Z_{eff}, P_{rad} or the central carbon concentration, fig 6.
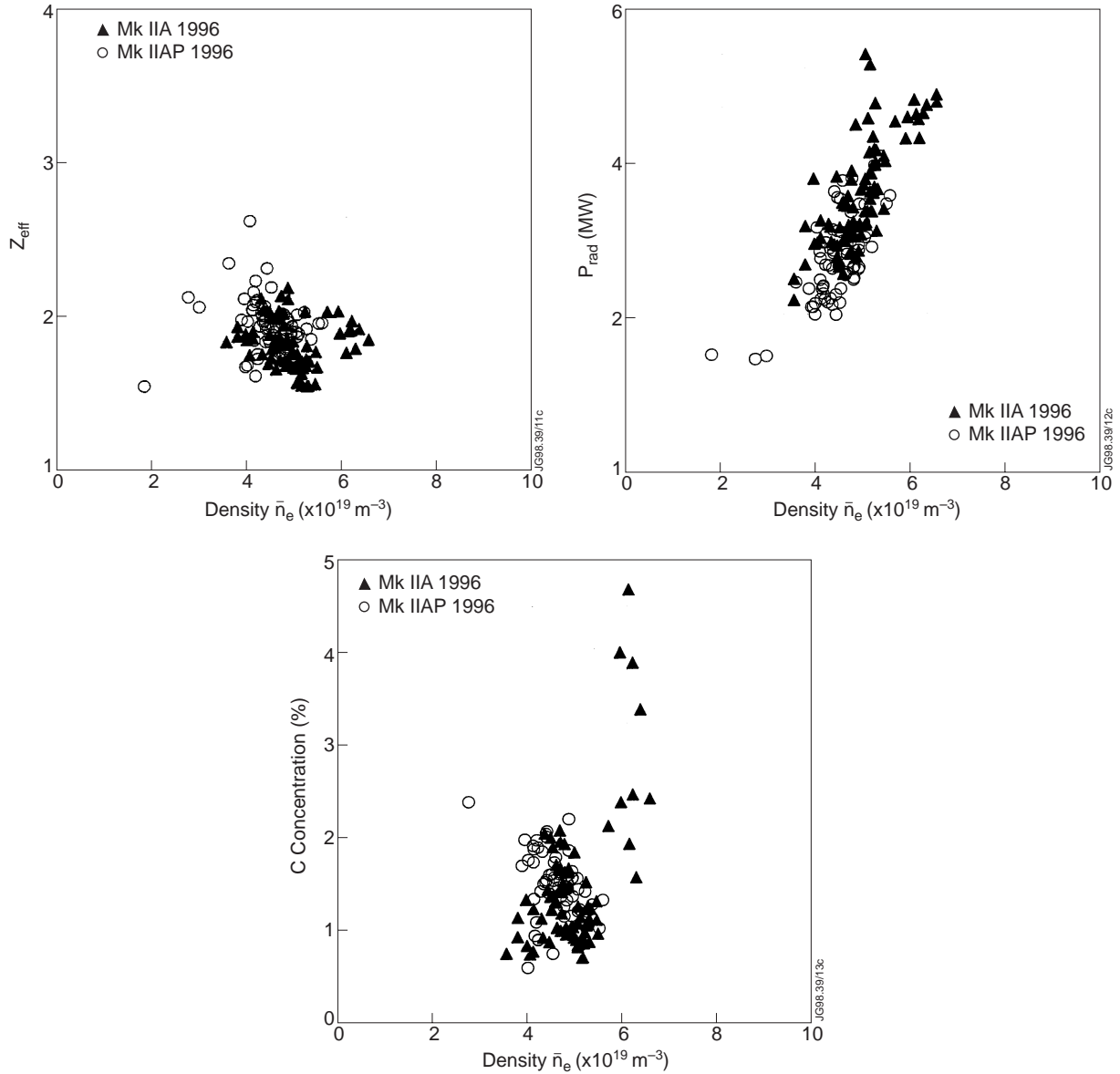

Fig.6: Comparison of the impurity levels in the MkII configuration before (Mk IIA) and after (Mk IIAP) the bypass leaks had been plugged.

(a) Zeff;

(b) Total radiated power.

(c) Carbon concentration at r/a=0.2;

Z_{eff} and P_{rad} data for MkIC, MkIBe and MkII are compared in figs 7a and 7b. For this comparison data have been selected with $10 < P_T < 14$ MW, corresponding to ELMy H-mode. Only low triangularity pulses (d < 0.25) have been included as the triangularity in Mk I was consistently lower than in Mk II. Mk IC has similar Z_{eff} and P_{rad} to Mk II but the Mk I data have a clearer trend of decreasing Z_{eff} with 'n_e and go to lower Z_{eff} at high density. The best shots in
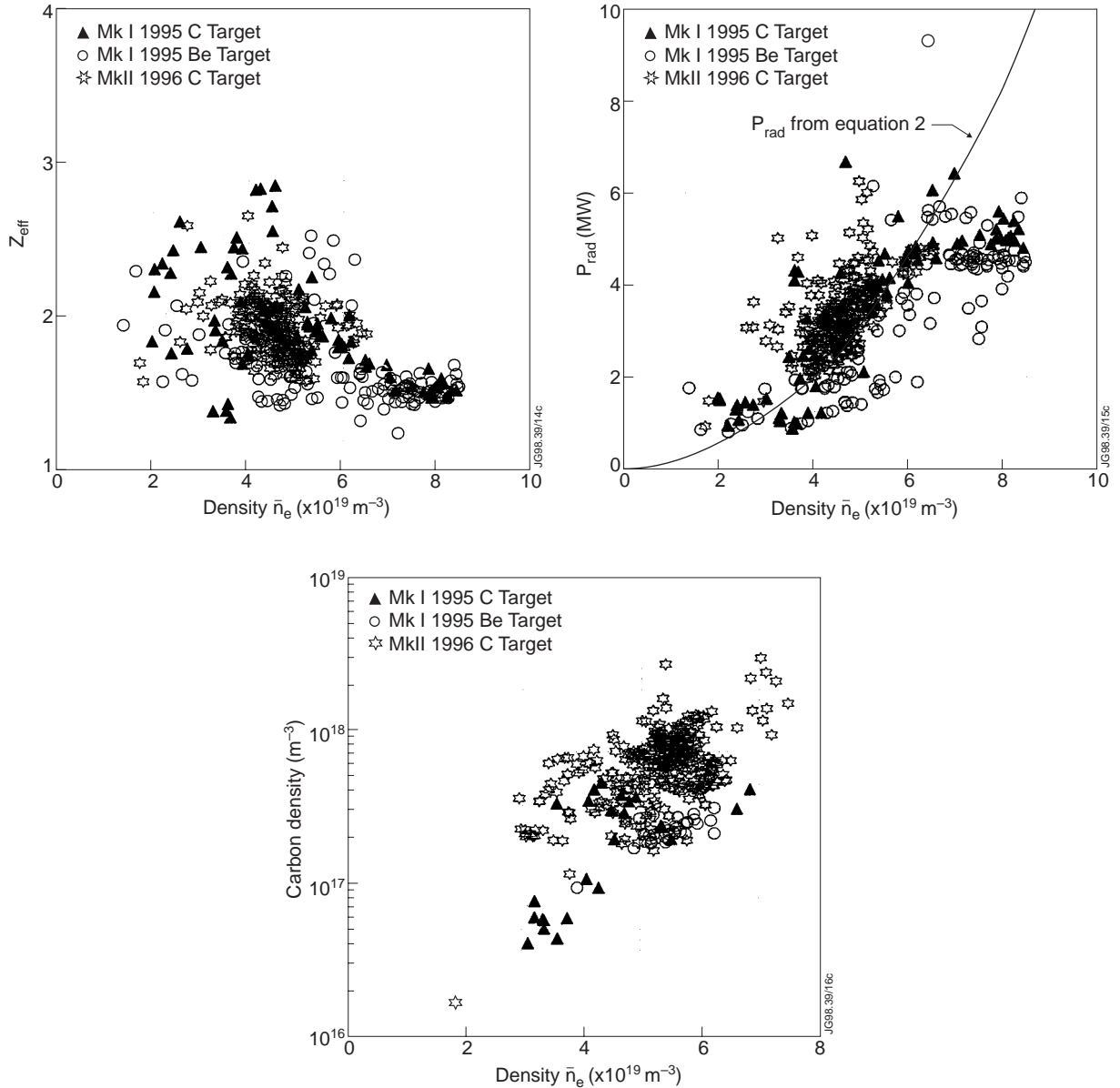
8

Fig.7: (a) Z_{eff} for different divertors, Mk IC, Mk IBe and Mk II during ELMy H-mode campaigns with core plasma density. Total input power P_T in the range 10 to 14 MW and with $2.4 < I_p < 2.7$ MA; Triangularity <0.25. No ICRH or LH heating. The target temperature in Mk I was ~ 400K and in Mk II it was 600 K.
(b) P_{rad} dependence on core plasma density, $\bar{n}_e$.
(c) C density vs $\bar{n}_e$.

MkII are just as good as in Mk IC up to a density '$n_e = 5 \times 10^{19}$ m^{-3}. Mk I Be has a Z_{eff} which is ≈ 0.3 lower than the carbon target cases over most of the density scan, but is similar to Mk IC at high density. P_{rad} is about 1 MW lower for the Be target than for the two carbon target campaigns. The 'n_e^2 scaling is not so clear as in fig 2d. This is partly because for a given power it is operationally difficult to get a large density range.

As with the global parameters, Z_{eff} and $P_{rad,}$ there is little difference between the carbon densities in Mk I, Mk II, figs 7c. The carbon concentration for the Mk I divertor with the carbon target is in the range 0.5-3%, similar to the results in fig 3a for Mk II. The beryllium concentra-

tion is generally less than 1% and is near to or less than the lower limit of detection. The Mk I campaign with the Be target had a significantly lower carbon concentration, consistent with the lower Z_{eff}, but the dominant impurity was still carbon. The carbon concentration was in the range 0.5 - 1.0%, i.e. approximately half that obtained with the carbon target. The Be concentration, measured by charge exchange, was not significantly larger than with the carbon target i.e. $\leq 1\%$.

2.3. Carbon influxes

The impurity influxes vary widely over the wall, limiter and divertor surfaces, depending on the incident flux and energy of the arriving plasma. The highest impurity flux density comes from the "wetted area" of the divertor plates where the scrape off layer (SOL) interacts with the target surface and where there is the highest incident plasma flux density. However, to estimate the contribution of different surfaces to the central impurity density, the surface interaction area and the transport of the impurity influx have to be taken into account.

A large number of low charge state impurities are routinely monitored with visible spectrometers using different viewing lines [19]. The diagnostics for the impurity and hydrogen recycling influxes are shown in fig 8. Spectroscopically resolved data in the visible are available from integrated views of both the inner and outer JET divertor targets, a horizontal midplane view of the inner wall, a vertical view of the outer wall above the outer target and 7 narrower angle views (30 mm wide at the target) (KS3). The main lines of sight are shown in fig 8. The spatial distributions of D_α, CII and bremsstrahlung (at 523 nm) across the inner and outer target are obtained, with 3 mm resolution at the target, from three flux cameras with interference filters, (KL2) [25].

The general trend of the CIII (465 nm) photon fluxes as a function of plasma density

Fig.8: Diagnostic lines of sight for monitoring the low charge state ions indicating impurity influxes. KS3 visible spectrometer, (inner wall, KS3 HOR, inner and outer targets, KS3INNER and KS3OUTER), and uv scanning mirror spectrometer, KT1.

is shown in fig 9a for the horizontal midplane view of the inner wall and for the inner and outer divertor targets during the 1996 Mk II campaign. The fluxes from the outer target are about a factor of 2 lower than the inner target, while the flux from the inner wall is about 2 orders of magnitude lower. The data shown are for neutral beam heating with total input power in the range $P_T = 10$ to 14 MW, corresponding to ELMy H-mode operation. However discharges with
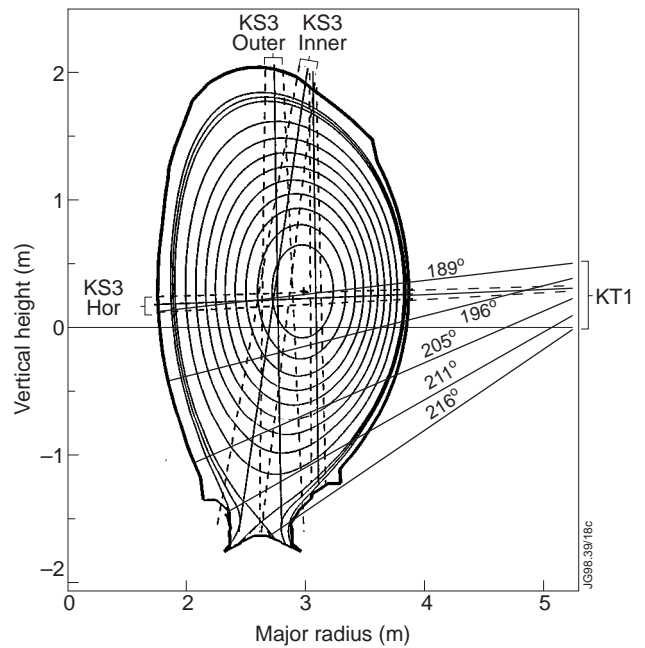
P_T = 4 to 8 MW, have similar fluxes. The photon yields, i.e. the ratios of the number of CIII photons to the D_α photons are shown in fig 9b for the same views as the photon fluxes. When the photon efficency is taken into account the estimated flux of carbon atoms is consistent with the total erosion of the inner wall integrated over a campaign using long term samples [26]. The photon yields in fig 9b drop markedly at a density of 5 to 6×10^{19} m^{-3}. This is due to the onset of recombination causing a rapid increase in the D_α flux at detachment [27].
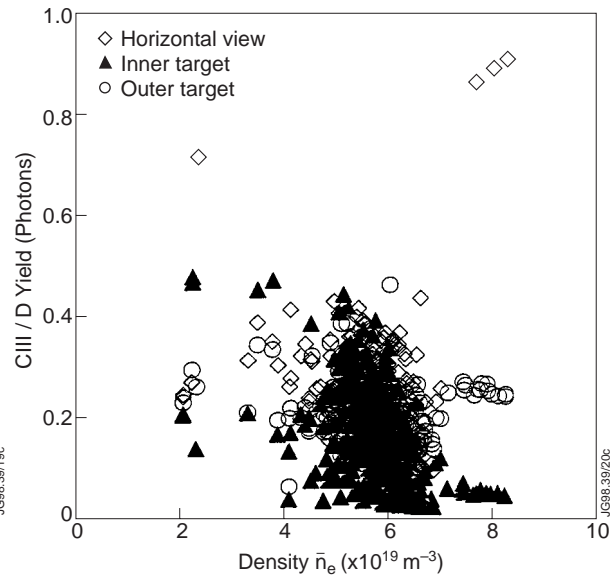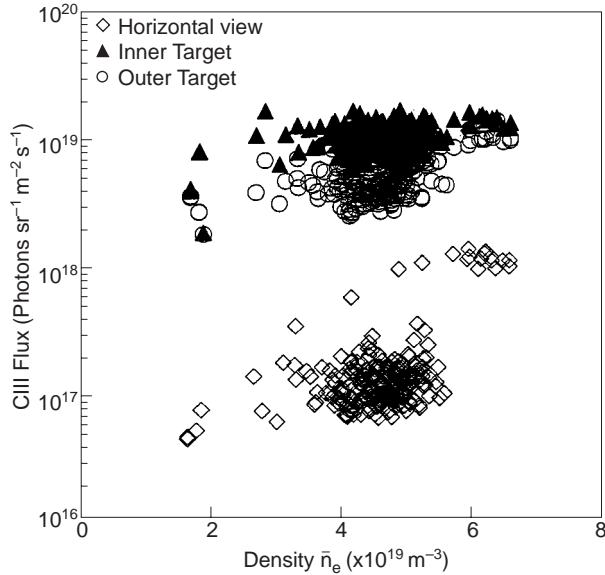

Fig.9a: Photon intensities of CIII (465 nm) from the horizontal mid plane view of the inner wall and from the inner and outer divertor targets during the 1996 Mk II campaign. Operating conditions, 2.4 MA < Ip < 2.7 MA, 10 MW < P_T <14 MW, diverted plasmas with triangularity δ < 0.25. No LH or ICRF heating

Fig.9b: Photon yields CIII/D_α for the same conditions and lines of sight as fig 9a.

The absolute CIII photon fluxes and the ratios of CIII/D_α as a function of density have been compared for different observation positions in the 3 campaigns, Mk IC, Mk IBe, and Mk II, fig 10a,b. The most reliable measurements are those at the outer target, as discussed above. The CIII/D_α ratio is a factor of 2 to 4 lower in the Mk I Be campaign than with the carbon targets, consistent with the Zeff measurements. The CIII/D_α ratio during the Mk II campaign is approximately a factor of 2 larger than during the Mk I with the carbon target. The difference is more marked at high density. While the higher photon ratio could be due to a lower value of T_e at the outer target in the MkII campaign, T_e would have to be lower by a factor 2 and there is no direct evidence for this being so. A possible explanation for the higher yield is that the CIII flux is dominated by chemical sputtering, which is qualitatively consistent with the higher target temperature during the Mk II campaign. The comparison between the MkIC and the Mk II is interesting in that although at $^{TM}n_e$= 4×10^{19} m^{-3} there is a factor 2 between them, the density dependence is stronger in the Mk IC than the MkII. As $^{TM}n_e$ increases the target plasma temperature is expected to fall, resulting in a lower ion energy incident on the target. Although both
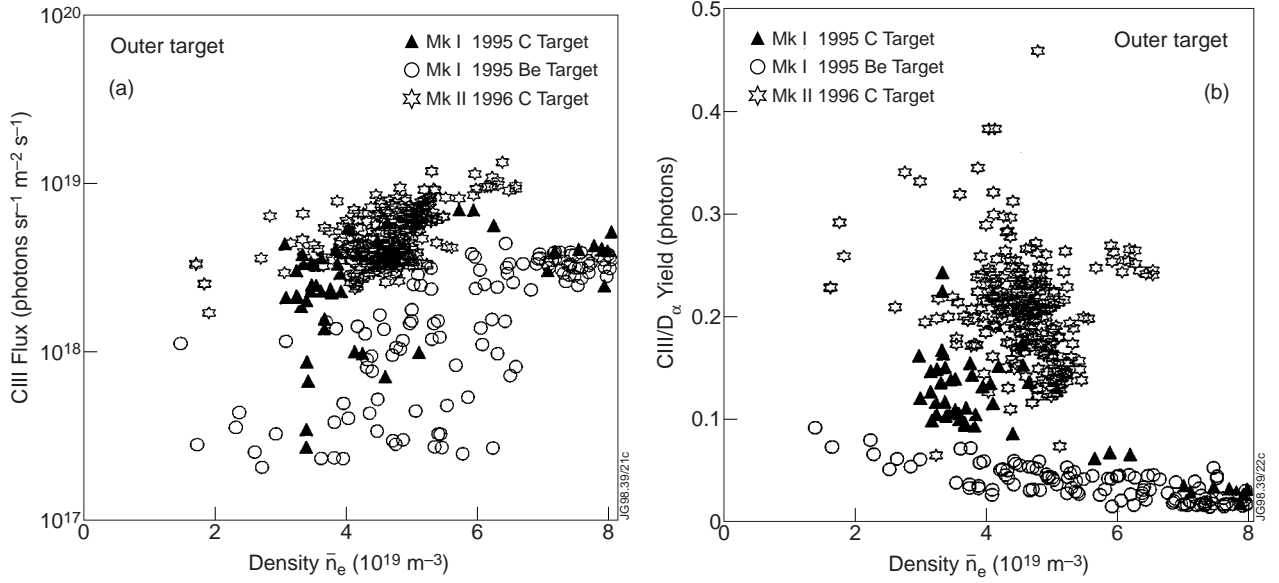
Fig.10: Comparison of (a) the photon flux from CIII (465.0 nm) and (b) the photon flux ratios CIII/D$_\alpha$ from the different divertors, Mk IC, Mk IBe and Mk II during ELMy H-mode campaigns. Operating conditions, Diverted plasmas with 2.4 MA < Ip < 2.7 MA, 10 MW < P$_T$<14 MW, and triangularity d < 0.25. No LH or ICRF heating

physical and chemical sputter yields decrease with decreasing energy, the effect is stronger with physical sputtering in this range of energy. Thus the difference in the behaviour in the two carbon campaigns could be due to enhanced chemical sputtering at the higher surface temperature of the Mk II target.

In order to derive particle influxes from the photon fluxes it is necessary to know the photon efficiency, defined as the number of photons per ionization event. These data are available from ADAS [28]. However the photon efficiency is a function of both the temperature and density at the position where the atom emits the photon. Thus to get a reliable measure of the particle influx it is necessary to know the T_e and n_e profiles reasonably accurately. The inverse photon efficiency (ionizations/photon, S/XB) is roughly linear with T_e in the range of interest. Photon flux ratios together with their appropriate S/XBs are tabulated in Table I, for some observed spectral lines for ELMy H-mode discharges in Mk IC, Mk IBe, Mk II. For each species the number of ions produced is the product of the photon flux and the S/XB. The most recent ADAS carbon data (C96) and the unresolved SXBs have been used. This implies that the metastable states are in equilibrium and that fluxes calculated from the doublet and quartet systems of the CII and the singlet and triplet systems of CIII should be the same. For the Mk II data, where most detailed reults are available, the agreement is reasonable and certainly with the scatter in the experimental photon yields. Given the scatter in the tokamak data and the uncertainties in the sputtering data, the yield, C/D=0.006 to 0.034 atoms /ion, could be explained by either physical or chemical sputtering [29, 30, 31]. The lower yield calculated for the CIII may be explained by loss of ions to the wall before ionization to CIII. Direct evidence of this shielding effect has previously been obtained using CCD cameras with CI and CII filters viewing either carbon sublimation at hotspots or injected CH_4. Carbon plumes flowing from the point of

12

injection towards the target have been observed and attributed to the frictional force of the background plasma [33]. The yield for the Mk IC campaign is lower than for the MK II as discussed above. The carbon yield for the Be target is even lower than either of the carbon targets, as expected, due to the low carbon density on the beryllium target.

Table I Average experimental yields of carbon from different sources in various charge states for ELMy H-mode discharges in Mk IC, Mk IBe, Mk II. $\bar{n}_e = 5 \times 10^{19} \, m^{-3}$, P_T = 10-12 MW, S/XB calculated for T_e =30 eV.						
	Species	Wavelength (nm)	S/XB	C/D_α (photons)	Yield (atoms/ ion)	
Mk II						
Outer Target	$CD^{(1)}$	431.0	120	0.008	0.024	
Outer Target	CII	426.7	35	0.015	0.013	$d^{(3)}$
Outer Target	CII	514.5	34	0.04	0.034	q
Outer Target	CII	657.8	16	0.04	0.016	d
Outer Target	CIII	465.0	1.55	0.2	0.008	t
Outer Target	CIII	569.7	287	0.0015	0.011	s
Inner Wall (midplane)	CIII	465.0	1.55	0.24	0.009	t
Inner Wall (above target)	CII	68.7	2.2	0.25	0.014	d
Mk IBe						
Inner Target	CIII	465.0	1.55	0.1	0.004	
Outer Target	CIII	465.0	1.55	0.06	0.002	
Mk IC						
Outer Target	CIII	465.0	1.55	0.15	0.006	
	$D_\alpha^{(2)}$	656.1	40			
	$D_{L\beta}$	102.5	32.2			
(1) There are no molecular data in ADAS and so the value obtained experimentally by Behringer for the CD molecule [32] has been used, although there is a caveat that these data are measured for much lower densities, ($\sim 1 \times 10^{18} \, m^{-3}$). (2) The S/XB for deuterium is 40, due to the high density assumed. (3) In the Mk II data the positions of the lines in the spectroscopic configuration are denoted thus: s,singlet, d, doublet, t,triplet, q, quartet. The SXB are unresolved.						

While relatively detailed measurements of the photon fluxes and plasma parameters have been made at the divertor and at the inner wall midplane, it has become increasingly evident that other impurity sources need to be considered. Impurities from the divertor strike points are expected to be rather well shielded from the core plasma since the impurity ionization length is less than that of the deuterium so that impurities are carried back to the target by the flow of the recycling deuterium [34]. Thus it is possible that lower fluxes from sources which are less well shielded, together with the larger surface area, may result in the wall being a more serious source of core contamination than the divertor targets. Early evidence from modelling [35], from other machines [4,8,36] as well as direct measurements of fluxes from the wall above the inner divertor in JET indicate that this is a potentially serious source of contamination. This was the basis for designing the Mk II divertor with the more closed geometry.

Measurements of the poloidal distribution of the carbon influx from the wall above the inner divertor have been made with a uv spectrometer using a rotating mirror. (KT1) [37]. While the database with this diagnostic is not as extensive as with the other spectroscopic measurements, data have been taken over a range of operating conditions. The poloidal profiles of carbon fluxes (CII, 68.7 nm), during typical H-mode and ohmic conditions are shown in fig 11a The carbon flux drops about an order of magnitude in going up the inner wall from the divertor to the midplane. The shapes of the distributions are similar for both phases with the H-mode data being a factor of about 5 times higher. Spatially, the flux is a maximum near the top of the vertical target, θ =210˚, cf fig 8. At larger angles, i.e. in the divertor, the spectrometer is vignetted and the signal drops. The carbon yields relative to $D_{L\beta}$, (102.5 nm), corrected for the photon efficiencies, are shown in fig 11b. The
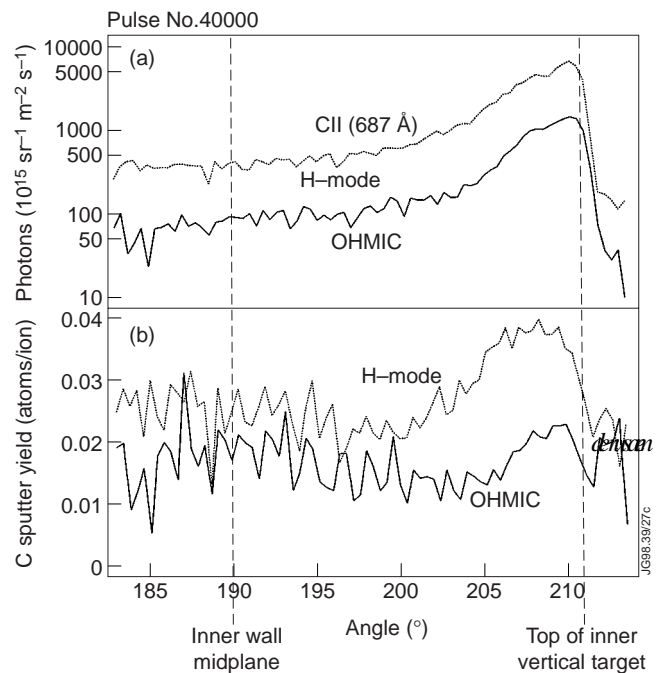

Fig.11: Poloidal distribution of CII (68.7 nm) photon flux from the inner wall above the inner divertor target, with the rotating mirror spectrometer KT1 (cf fig 8). Plasma conditions shot 40000, Ip =2.5 MA, B_t = 2.5 T, $\overline{n}_e$ =1.3x10^{19} m^{-3}, (ohmic) and $\overline{n}_e$ =5.2x10^{19} m^{-3}, (H-mode). P_T= 12 MW . Note that θ=190˚ corresponds to the inner wall midplane position because the spectrometer viewing point is above the midplane.

deuterium line was measured simultaneously on a second channel of the spectrometer. The yields vary little with angle and are ~ 0.017±0.005 for the ohmic phase and 0.026± 0.005 for the H-mode phase. The photon efficiencies for these lines should be reliable as they both involve transitions to the ground state. The atom yields at the midplane (θ =190˚) are in good agreement with the values obtained from the visible spectrometer (CIII, 465.0 nm) at the inner midplane, Table I

14

2.4. Beryllium fluxes

Due to the use of routine beryllium evaporation for gettering, beryllium influxes have been observed in all phases of the divertor program, both in Mk I and Mk II. The beryllium fluxes are monitored using the same lines of sight as used for the carbon fluxes. The photon yields from the horizontal view, the inner and the outer targets during the Mk IBe campaign, are shown for the Be II (527 nm) line in fig 12a. The photon fluxes from the inner and outer targets are the same within the scatter of the data, $\sim 3 \times 10^{13}$ photons m^{-2} sr^{-1} s^{-1} for medium densities, $\bar{n}_e \sim 5 \times 10^{19}$ m^{-3}, while the flux from the horizontal midplane is more than an order of magnitude smaller. The absolute values of the photon fluxes are much lower than for CIII simply because the photon efficiency of the BeII line is lower. The flux from the divertor targets is decreasing with increasing density while the flux from the inner wall is clearly increasing with density, so that at the highest densities the fluxes are within a factor of 3. The photon yields, i.e. the BeII fluxes divided by the D_α photon fluxes, are compared in fig 12b for the same views. The yields from the divertor targets are again similar and about an order of magnitude higher than the yield from the inner wall. This is consistent with the targets being solid beryllium while the inner wall is only partially covered with evaporated beryllium. The BeII photon yields from the targets in the campaigns with carbon targets are also an order of magnitude lower than those from solid beryllium.
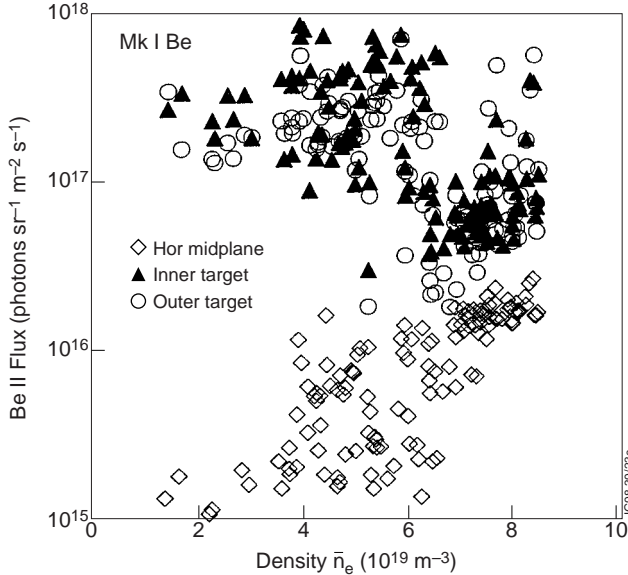

Fig.12a: Photon intensities of BeII (527.1 nm) from the horizontal mid plane view of the inner wall and from the inner and outer divertor targets during the 1995 Mk IBe campaign. Operating conditions: Diverted plasmas with 2.4 MA < Ip < 2.7 MA, 10 MW < P$_T$ <14 MW, and triangularity d < 0.25. No LH or ICRF heating
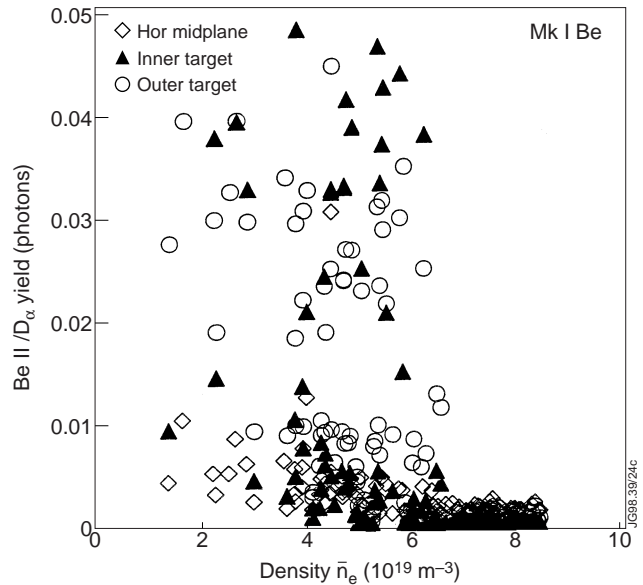
Fig.12b: Photon yields BeII/D$_a$ for the same conditions and lines of sight as fig 12a.

The beryllium influx and the photon yields in the 3 campaigns Mk IC, Mk IBe and Mk II are compared in fig 13, for the outer divertor. The data are very scattered but the Mk IC data are much lower than the Mk IBe and the Mk II. The fluxes appear to be decreasing with increasing density for Mk IBe. For the carbon target cases the fluxes are too scattered to see any clear trend. The photon yields Be II/D_α are compared in fig 13b. This shows that although the absolute Be II fluxes are similar for Mk IBe and Mk II. fig 13a, the yields are consistently lower, as expected. The Mk IC yields are lower than Mk II.
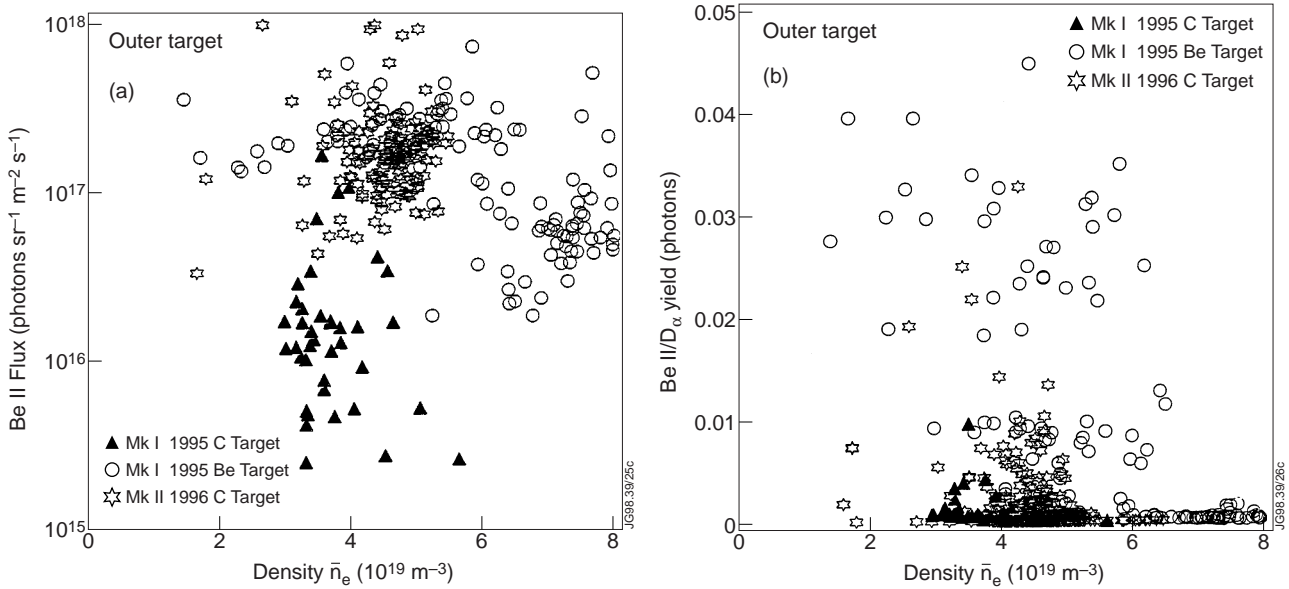

Fig.13: Comparison of (a) the photon flux from BeII (527.1 nm) and (b) the photon flux ratios BeII/D_α, from the different divertors, Mk IC, Mk IBe and Mk II during ELMy H-mode campaigns, P_T=10-12 MW. Operating conditions: Diverted plasmas with 2.4 MA < Ip < 2.7 MA, 10 MW < P_T <14 MW, triangularity d < 0.25. No LH or ICRF heating

The photon yields have been corrected for the photon efficiencies in a similar way to the carbon data, in Table II. The same target plasma temperature and density have been assumed as for the carbon fluxes. The estimated sputter yield for the beryllium targets is 0.06 atoms/ion. This is in reasonable agreement with both experimental and theoretical sputter yields for deuterium ions normally incident on beryllium at energies above 100 eV [29]. The results for the inner and outer targets are similar. In all cases the yield Be/D decreases rapidly above a density $\bar{n}_e > 5 \times 10^{19}$ m^{-3}. The fall could be explained by the decreasing physical sputter yield as the density increases and the ion energy decreases to near or below the threshold for physical sputtering but, as in the case of the carbon, it is more likely due to the increase in the D_a radiation as the targets become partially detached and recombination radiation becomes dominant. The effective Be sputter yields estimated for the carbon targets are ≤ 0.005 atoms/ ion. The yields for the inner and outer targets and midplane view are all similar. While there is no way of estimating what this yield should be, it is consistent with a low beryllium coverage of the carbon targets. No measurements have yet been made of the beryllium fluxes from the wall above the inner target.

16

	Species	Wavelength (nm)	S/XB	Be/Dα (photons)	Yield (atoms/ ion)
Table II Average experimental yields of beryllium from different sources for ELMy H-mode discharges in Mk IC, Mk IBe, Mk II. $\bar{n}_e = 5 \times 10^{19}$ m^{-3} , P_T=10-12 MW, S/XB calculated for T_e =30 eV.					
Mk II					
Outer Target	BeIa	440.8	1300	0.01	0.325
Outer Target	BeIb	447.3	35	0.006	0.005
Outer Target	BeIIa	527.1	60	0.004	0.006
Outer Target	BeIIb	436.1	20	0.01	0.005
Outer Target	BeIIc	467.3	9	0.005	0.001
Outer Target	BeIId	482.9	60	0.01	0.015
Inner Wall	BeIIa	527.1	60	0.004	0.006
Mk IBe					
Hor. Midplane	BeIIa	527.1	60	.015	0.023
Inner Target	BeIIa	527.1	60	.04	0.06
Outer Target	BeIIa	527.1	60	.04	0.06
Mk IC					
Inner Target	BeIIa	527.1	60	.004	0.006
Outer Target	BeIIa	527.1	60	.002	0.003

3. DISCUSSION

3.1. Z_{eff} and P_{rad}.

From their definitions it is possible to derive a simple relation between Z_{eff} and P_{rad} for a simple 0-D plasma model.

$$P_{rad} = (Z_{eff} - 1)™n_e^2 \, L(T_e) \, V/Z(Z-1) \qquad (1)$$

where $L(T_e)$ is the radiation constant, which is a function both of T_e and of impurity confinement time, V is the radiating volume and Z is the charge of the impurity. The relationship derived from a regression analysis of this parametric dependence for a number of tokamaks for the ITER database gives [38]

$$P_{rad}=0.18(Z_{eff}-1)^{TM}n_e^{1.95\pm0.04}S^{1.02\pm0.02}/Z^{0.19\pm0.05} \tag{2}$$

where S is the surface area of the plasma and a radiating layer of constant thickness is assumed.

The result from eqn(2) is plotted in fig 2d and is seen to be consistent with the general trend of the experimental data in the figure. Comparing eqn (1) with eqn (2) implies a value of $L(T_e).V=5\times10^{-32}$ W m^6 which is consistent with a value of $L(T_e)=5\times10^{-33}$ W m^3 and V= 10 m^3. This value of $L(T_e)$ is consistent with calculated values for carbon within the uncertainty in T_e.

3.2. Time correlation of impurity influxes with core impurity density.

The impurity fluxes from the various plasma facing surfaces of the tokamak must together be responsible for the central impurity density. It is thus useful to compare the individual influxes measured experimentally with the central carbon concentration in order to find out if there is any correlation, and possibly determine the source of the impurities that contaminate the plasma.

Let us consider a simple analytical model to calculate the central carbon density from the carbon influxes, using a global impurity confinement time. The relation between the incoming impurity flux densities, $\Gamma_i(t)$, and the central density $n_z(t)$ can be written.

$$n_z(t) = \sum_i F\big(\Gamma_i(t), A_i, \tau_z\big) \tag{3}$$

where A_i is the area of the source i, and τ_z is the impurity confinement time. The screening probability has to be determined and in general this can only be done by detailed 2-D modelling, either fluid or Monte Carlo.

If a global model is assumed for the time dependence of the confined impurities, then

$$\frac{Vdn_z(t)}{dt} = -\frac{Vn_z(t)}{\tau_z} + \sum_i A_i\Gamma_i(t) \tag{4}$$

The τ_z in equation (4) is the true particle confinement time and is influenced as much by the edge as the core transport. Often τ_z is much shorter than the characteristic time for filling or emptying the core plasma, τ_c. It is useful therefore to introduce screening probabilities f_i such that the fuelling rate of the core reservoir is defined to be $\sum A_i f_i \Gamma_i$ and to then replace τ_z by τ_c. The solution to equation (4) for the situation when only a single source is present is:

$$n_z(t) = \frac{f_iA_i}{V}\exp(-\frac{t}{\tau_c}).\int_0^t \Gamma_i(t).\exp(\frac{t}{\tau_c}).dt. \tag{5}$$

18

If we now consider the individual sources for which there are experimental data, τ_c and f_i can be fitted to obtain a good match to the time evolution and the central carbon density. In this way it may be possible to see if individual sources are consistent with the central density.

An example of this exercise is shown in fig 14 for an L-mode discharge. The particle influxes from the inner wall and the inner and outer targets are shown separately.These fluxes have each been integrated to derive the core impurity density using eqn (5) and the 2 fitting factors τ_c and f_i . The experimental impurity carbon density is derived from the charge exchange diagnostic and is only available when the neutral beams are on. The value of τ_c that best fits the three cases is 0.3 s and it is seen that the three impurity source functions have similar time dependencies. Thus it is not possible to distinguish between the sources on this basis. The value of the impurity confinement time obtained is comparable with τ_E, which is
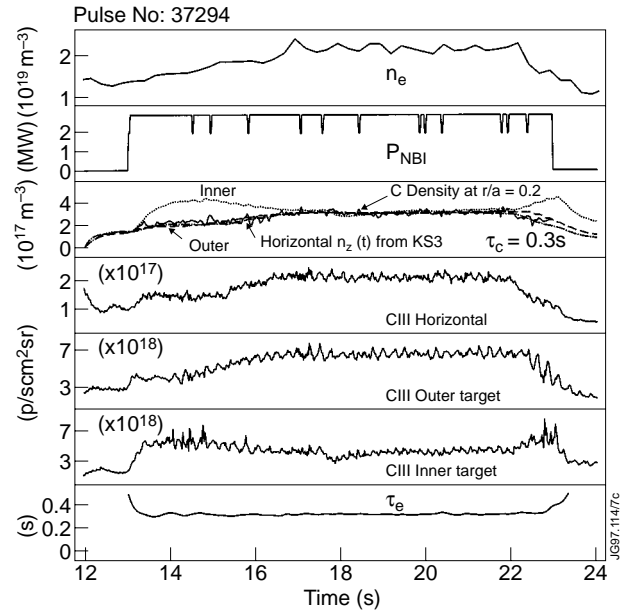
typically 0.35s for these L-mode discharges.

Fig.14: Comparison of the central carbon density (at r/a=0.2), measured with the charge exchange diagnostic, with the density derived from the measured impurity influxes (KS3 spectrometer)using the global model in equation 5. A low triangularity L-mode discharge (37294), with horizontal target and high flux expansion. The impurity confinement time, t_c, derived is 0.3 s. and the

An example of an ELMy H-mode is shown in fig 15. Here the central carbon density is calculated by integrating the influx from the inner wall below the midplane as measured with the KT1 spectrometer. The derived value of τ_c in this case is 1.0 s Again a reasonably good agreement is obtained between the measued carbon density and the value calculated from the influx. A third example is shown in fig 16 for an H-mode discharge with a low ELM frequency; the fluxes from the divertor targets and the inner wall midplane are integrated. The fitted value of τ_c is now ~ 10 s. The time dependence of the impurity fluxes from different sources is similar. This is not surprising as they are all determined by the particle and energy flux flowing in the SOL. It seems clear that for a particular discharge the impurity density in the core is consistent with the influxes, even it is not possible to distnguish between the effect of the different sources separately. The remarkable result is that the effective impurity confinement time varies so widely in different types of discharge. This means that it is impossible to get any meaningful correlation between influxes and central densities without taking the change in τ_c into account. The derived values of τ_c in H mode can be factors of 3 to 30 higher than the experimentally measured τ_E .
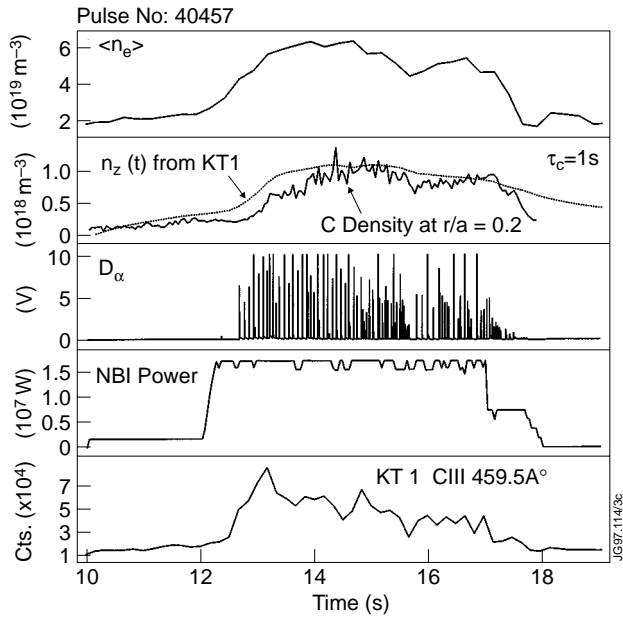
Fig.15: Comparison of the central carbon density (at r/a=0.2), measured with the charge exchange diagnostic, with the density derived from the measured impurity influxes from the inner wall (KT1 spectrometer) using the global model in equation 5. A low triangularity H-mode discharge (40457), with horizontal target and high flux
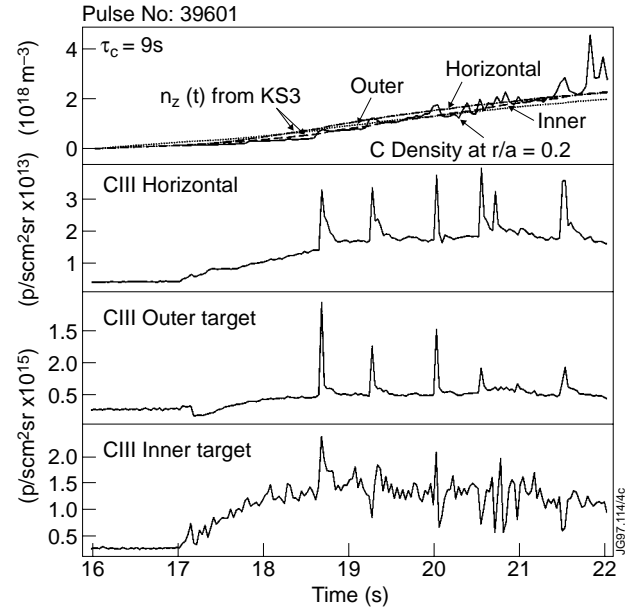
Fig.16: Comparison of the central carbon density (at r/a=0.2), measured with the charge exchange diagnostic, with the density derived from the measured impurity influxes (KS3 spectrometer)using the global model in equation 5. A high triangularity H-mode discharge (39601), with

horizontal target and high flux expansion. The impurity confinement time, t_c, derived is 9 s.

3.3. Intensity correlation of impurity influxes with core impurity density

The absolute carbon photon fluxes have been compared to the central impurity density in fig 17 for ELMy H-mode in the Mk II campaign with $10 < P_T < 14$ MW. The selection has been limited to discharges with low triangularity in order to minimize the variation in τ_c. One might hope that there would then be a correlation between the influxes and core impurity density. Unfortunately because of the large scatter in the data it is difficult to see any clear dependence of the core density on the influx. The scatter is partly because of the random occurrence of ELMs and because the data in the data base does not record whether there is an ELM. The fact that a wide range of densities and powers has been included also contributes to the scatter. Data for ohmic and L-mode with neutral beam powers up to 6 MW (not shown) have fluxes a factor of 2 to 3 lower and are slightly less scattered. The average photon fluxes, normalized to a central carbon concentration of 1×10^{18} m^{-3}, and the corresponding ion fluxes are shown in Table III. The same values of S/XB have been used for all geometrical views and the flux densities have been multiplied by the total area viewed, assuming the radiation to be toroidally symmetric. Of course such estimates of fluxes are only order of magnitude since the values of the S/XBs are obtained

20

for rather arbitrary edge plasma parameters, but the consistency of the sputter yields calculated in Tables I and II give some degree of confidence. The fluxes from the inner and outer targets are the same order of magnitude, while the fluxes for the horizontal midplane are at least an order of magnitude lower.

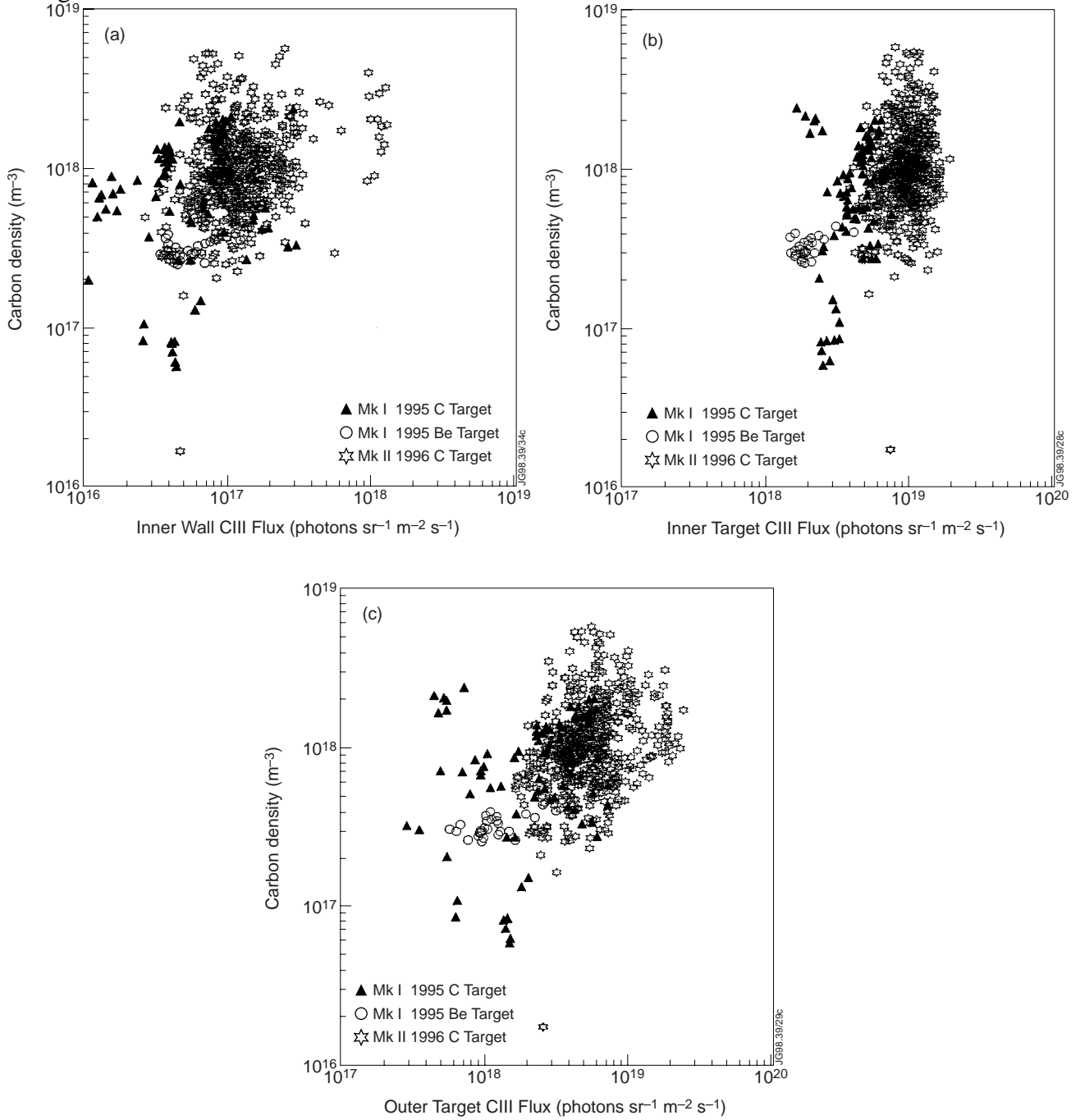*Fig.17: Comparison of the photon fluxes from CIII (465.0nm) in the three campaigns for different divertors, Mk IC, Mk IBe and Mk II, with the core carbon density measured by charge exchange at r/a=0.2. Total input power P_T in the range 10 to 14 MW with $2.4 < I_p < 2.7$ MA; Triangularity <0.25; no ICRH or LH heating.*
(a) Horizontal midplane CIII photon flux, (b) Inner target CIII photon flux, (c) Outer target CIII photon flux.

Species	Wavelength (nm)	Photon Flux (photons/m²/sr/s)	S/XB ions/phot	Area m²	Atom Flux/s	Screen Factor
Table III Average experimental fluxes of carbon and beryllium from different sources corresponding to an impurity density of 1×10^{18} m^{-3} at r/a=0.2 for ELMy H-mode discharges. $\bar{n}_e = 5 \times 10^{19}$ m^{-3} , P_T=10-12 MW, S/XB calculated for T_e =30 eV. The plasma volume is assumed to be **80 m^3** and the core impurity confinement time τ_c = 1.0 s.						
Mk II						
CIII (hor)	465.0	1×10^{17}	1.55	38	7.4×10^{19}	1.1
CIII (inn. tgt)	465.0	8×10^{18}	1.55	6.4	1.0×10^{21}	0.08
CIII (out. tgt)	465.0	4×10^{18}	1.55	5.8	4.5×10^{20}	0.18
CII (inner. wall)	68.7		2.2		4.4×10^{20}	0.18

If we consider steady state conditions and consider that each source is responsible for the central impurity density in turn we obtain from eqn (4) that the screening factor for source i is given by

$$f_i = \frac{1}{A_i \Gamma_i} \frac{V n_z}{\tau_c}$$

By assuming a value for τ_c and considering each of the sources individually as the sole source of the central impurity we can calculate the effective screening factor f_i for that source. The screening factors for carbon, obtained for each of the source positions, assuming $\tau_c = 1.0$ s, obtained for an H-mode with ELM frequency >20 Hz, are given in Table III. It is seen that for carbon $f_i \sim 0.1$ for the inner and outer divertor fluxes, whereas the flux from the inner wall midplane has $f_i \sim 1.0$, i.e. it is insufficient to account for the core density unless all the impurity atoms enter the confined plasma. The higher estimated flux for the inner target is probably because of the incorrect assumption that T_e at the inner and outer targets are the same. Over a wide range of discharges the fluxes from the inner and outer targets are usually within a factor of 2. If less than 10% of the impurities from these two sources entered the plasma they would be enough to account for the core impurity density.

We also have the measured fluxes from the rotating mirror spectrometer (KT1) presented in fig 11. The poloidal profiles have been integrated over the area of the inner wall above the inner target up to the midplane. Because of the substantial contribution from the wall immediately above the target the total flux is comparable to that from the divertor targets themselves. The screening factor has been calculated for a limited number of H-mode discharges to be ~0.1 using the measured carbon content for each discharge. It has been found from Monte Carlo calculations that the screening of impurities from the inner wall is much less effective than from the target because the friction with the background gas is much lower than it is near the target

[34,35]. Thus the high absolute impurity influx from this region must be a strong candidate for contributing to the central impurity density

It is noted that while the carbon fluxes are a factor of 2 higher in the Mk II than the Mk IC divertor, the beryllium fluxes are a factor of 10 higher in the Mk IBe divertor than the Mk IC or Mk II divertors. When the Be flux is high in the Mk IBe divertor the corresponding C flux is low, as expected.

4. CONCLUSIONS

Carbon is the main impurity under most operating conditions, with a concentration in the range ~ 1 to 3%, depending slightly on input power, configuration and gas flow rate. Nickel (the main metal impurity) is normally negligible. Other intrinsic impurities which make contributions to Z_{eff} and radiation occasionally are oxygen, chlorine and beryllium. The oxygen and chlorine occur when the machine is insufficiently conditioned and the beryllium can be significant for one or two shots immediately after Be evaporation. There was no effect on the central impurity densities (C or Ni) due to plugging the divertor bypass leaks in the Mk II divertor configuration. Mk IC results are similar to Mk II. However the Mk IBe has lower Z_{eff} and P_{rad}. The dominant impurity with the MkI Be targets is still carbon [6], with Be concentrations being typically ≤1%. This may be due to the Be targets becoming contaminated with carbon or to the principal source of the carbon coming from the walls of the main chamber.

The Z_{eff} is generally consistent with the measured carbon concentrations. The Z_{eff}, core carbon concentration and impurity influx are curiously independent of either input power or plasma density. The radiation increases approximately as $^{TM}n_e^2$, which is consistent with the constant Z_{eff} and carbon concentration. Quantitatively the radiation level implies a radiation constant $L(T_e) = 5 \times 10^{-33}$ watt m^3 which is consistent with the atomic physics data for carbon within the uncertainty in the electron temperature.

The core impurity density is strongly correlated with ELM frequency. This effect is independent of whether the ELM frequency is changed by varying the triangularity of the magnetic surfaces, the rate of fuelling or in other ways. In high triangularity discharges, with ELM frequencies ~ 5Hz, the nickel concentration increases to ~2×10^{-4}. This appears to be due to metal injection by large ELMs and to impurity accumulation during the ELM free periods. The high particle confinement associated with low ELM frequency in long pulse discharges can result in carbon concentrations ~3%, equivalent to nearly 20% dilution.

Considering the carbon impurities for conditions of low triangularity, i.e. an ELM frequency greater than 25, the impurity photon flux from the inner wall midplane and from the targets is observed to be almost independent of of density and input power. The fact that the core concentration is also constant implies that the effective integrated screening probability does not vary with plasma operating conditions. The yields of carbon atoms per incident deuterium ion are consistent with sputtering, either physical or chemical or a combination of the two. From the

dependence of the impurity density on the ELM frequency and from the correlation of the impurity density with the time evolution of the impurity influxes it seems conclusive that the impurity density is strongly dependent on the effective impurity particle confinement time, τ_c. τ_c varies considerably, in the range 0.3 to 10 s, leading to marked changes in the core impurity density. Examination of the time evolution of the impurity influx indicates that the carbon influx bursts during ELMs do not make a significant contribution to the core impurity density.

The time evolution of the influxes from the targets and the inner wall midplane are similar and all of them appear consistent with the evolution of the core impurity density. It is thus difficult to determine in this way which of them, if any, are the dominant sources contributing to the central density. The fluxes from the inner and outer target would be sufficient to explain the core density if ~ 10% of the primary flux crossed the separatrix. However, the similarity of the time dependence and the fact that, within the uncertainties in the estimates, any one of the sources might explain the central impurity density, illustrates how difficult it is to understand the impurity behaviour.

At present the strongest candidate for explaining the central impurity concentration is the impurity flux from the inner wall below the midplane. The spatially integrated flux is comparable with that from the inner and outer targets. The screening of impurities from this source is expected to be less effective than at the divertor targets due to the reduced frictional force of plasma flowing to the target. Further measurements of this source are clearly desirable over a wider range of operating conditions. Only about 20% of the source has to enter the plasma in order to account for the central concentration. Whether a screening factor of ~ 0.1 is realistic has not been addressed in the present analysis and will have to be answered by detailed modelling. More emphasis on modelling the impurity flux from the inner wall is necessary. This has tended to be neglected because of the difficulty of generating computational grids in the region close to the walls in the main chamber.

ACKNOWLEDGEMENTS

REFERENCES

[1]   Stangeby, P.C., and McCracken, G. M. Nucl. Fusion **30** (1990) 1225.

[2]   Eckstein, W., Bohdansky, J., and Roth, J., Atomic and Plasma Material Interaction Data for Fusion Nuclear supplement v 1 (1991) 51, IAEA Vienna.

[3]   Roth, J., Vietzke, E., and Haasz, A.A., Atomic and Plasma Material Interaction Data for Fusion Nuclear supplement v 1 (1991) 51, IAEA Vienna.

[4]   Fussman G, J. Nucl. Mater., **145-147** (1987) 96

[5]   Stangeby, P. C., and Elder, D., Nucl. Fusion **35** (1995) 1391.

[6]   Smith, G.R., Brown, P.N., Campbell, R.B., et al J Nucl. Mater., **220-222** (1994) 1024.

[7]   Taroni, A., Corrigan, G., Horton, L.D., et al, Plasma Physics and Controlled Fusion, Proc of the 22nd Eur. Phys. Soc. Conf, Bournemouth, IV (1995) 297.

[8]   Kallenbach, A., et al, Nucl. Fusion **34** (1994) 1557.

[9]   Janeschitz G., Pacher, H.D., Federicic, G., et al, Plasma Physics and Controlled Nuclear Fusion Research (Proc of the 16th IAEA Conf, Montreal,**2** (1996) 755 IAEA-CN-64/F-2) IAEA Vienna, 1997.

[10]   Pick, M.A., Decksnis, E., Dietz, K.J. et al J Nucl. Mat., **196-198** (1992) 215

[11]   JET Joint Undertaking Annual Report 1996, p60, EUR17620 EN-C, EUR-JET-AR19, May 1997

[12]   Lowry, C.G. Campbell, D.J., Davies, S.J., et al J Nucl. Mat., **241-243** (1996) 439

[13]   Vlases G.C. Plasma Physics and Controlled Nuclear Fusion Research (Proc of the 16th IAEA Conf, Montreal) 1 (1996)371) IAEA Vienna, 1997

[14]   Horton, L.D., Vlases, G.C., Andrew, P., et al, Nucl. Fusion companion paper to be published, 1998

[15]   Matthews, G.F., Balet, B., Cordey, J.G., et al , Nucl. Fusion companion paper to be published, 1998.

[16]   Thomas P.R. and the JET team, J. Nucl. Mater. **176-177** (1990) 3.

[17]   Campbell D.J. and the JET team J. Nucl. Mater. **241-243** (1997)379-384

[18]   McCracken, G.M., Guo, H.Y., Barnsley, R. et al, Plasma Physics and Controlled Fusion, (Proc of the 24th Eur. Phys. Soc. Conf, Berchtesgaden), 1 (1997) 57.

[19]   Behringer, K., Carolan, P.G., Denne, B. et al Nucl. Fusion **26** (1986) 751.

[20]   Mast, K.F., and Krause, H., Rev. Sci. Instrum. **56** (1985) 969; Reichle,R, Bartlett, D.V., Campbell, D.J., et al Plasma Physics and Controlled Fusion, Proc of the 22nd Eur. Phys. Soc. Conf, Bournemouth , III (1995) 085.

[21]   von Hellermann M.G., and Summers, H.P., "Active Beam Spectroscopy in JET" in Atomic and Plasma Materials Interaction Processes in Controlled Thermonuclear Fusion, Ed. Janev, R.K., and Drawin, H.W., Elsevier 1993, p135.

[22]   Bartiromo, R., Bombarda, F., Gianella, R., et al, Rev. Sci. Instrum. **60** (1989) 237.

[23]   Barnsley, R., et al Rev. Sci. Instrum. **57** (1986) 2159.

[24]   Mohanti, R., Brickley, C., Christiansen., J.P., et al Plasma Physics and Controlled Fusion, (Proc of the 24th Eur. Phys. Soc. Conf .,Berchtesgaden), 1 (1997) 101.

[25]   Lingertat, J., Tabasso, A., Ali-Arshad, S., et al, J Nucl. Mater. **241-243** (1997) 402.

[26]   Mayer, M., Behrisch, R., Andrew, P., and Peacock, A.T., J Nucl. Mater. **241-243** (1997) 469.

[27]   McCracken, G.M., Stamp, M.F., Monk, R.D., et al Nuclear Fusion **xx** (1998) xxx to be published

[28] Summers, H.P., Atomic Data and Analysis Structure Users Manual JET IR(94) 06

[29] Eckstein, W., Garcia-Rosales, C., Roth, J., and Ottenberger, W., Sputtering Data, Max Planck Institut, Garching, Report IPP 9/82, 1993

[30] Roth J., and Garcia-Rosales C., Nucl. Fusion, **36** (1996) 1647

[31] Mech, B.V., Haasz, A.A., and Davis, J.W., J Nucl. Mater. **255** (1998) 153.

[32] Behringer, K., J. Nucl. Mater. **176/177** (1990) 606.

[33] Lingertat, J., et al, Paper presented at the American Physical Society meeting, Seattle, Wash, 1992 JET IR (92)09, p31.

[34] Stangeby P.C., and Elder D., Nucl. Fusion, **35** (1995)1391.

[35] Matthews, G.F., Stangeby, P.C., Elder J.D., et al, J Nucl Mater. **196-198** (1992) 374.

[36] Hill D.N., Petrie,T.W., Allen, S .L., et al Plasma Physics and Controlled Fusion (Proc of the 20th Eur. Phys. Soc. Conf .,Lisbon ,1993), II (1993) 643.

[37] Chabert P., Breton, C., DeMichelis, C., et al., Contr. Fusion and Plasma

Physics, (Proc of the 16th Eur. Phys. Soc. Conf .,Venice ,1989), IV (1989)1505.

[38] Matthews G.F., Allen, S., Asakura, N., et al J Nucl. Mater. **241-243** (1997) 450.